*Materials Science-Poland, 34(1), 2016, pp. 53-62*
*http://www.materialsscience.pwr.wroc.pl/*
*DOI: 10.1515/msp-2016-0009*

DE GRUYTER OPEN

# Effects of thermal treatment and fluoride ion doping on surface and catalytic properties of NiO–$ZrO_2$ catalysts

REHAM M. ABDEL FATTAH[1]*, HALA A. KIWAN[1], AWAD I. AHMED[2], MOHAMED R. MOSTAFA[1]

[1]Chemistry Department, Faculty of Science, Damietta University, Damietta, 34517, Egypt
[2]Chemistry Department, Faculty of Science, Mansoura University, Mansoura, 35511, Egypt

$ZrO_2$ and a series of NiO/$ZrO_2$ hydrogels (5 to 25 wt.% NiO) were co-precipitated with the aid of NaOH–$Na_2C_2O_4$ solution. Two fluorinated hydrogels were also prepared by wet impregnation method. The samples were calcined in the temperature range of 550 to 850 °C. The surface properties of the samples were determined using DTA, XRD and nitrogen adsorption at −196 °C. The conversion of isopropanol was tested using microcatalytic pulse technique. DTA measurements showed that the addition of nickel oxide to zirconia influences the phase transition of $ZrO_2$. XRD revealed that the tetragonal phase was formed at T ⩽ 650 °C, while a biphasic mixture was obtained at T ⩾ 750 °C. No spinel structure was detected by both DTA and XRD techniques and only traces of cubic NiO were detected for the samples containing ⩾ 15 wt.% nickel oxide and calcined at T ⩾ 750 °C. Significant changes in texture, surface acidity and catalytic activity were found as a result of the effects of thermal treatment and chemical composition. Incorporation of fluoride ions greatly increased the surface acidity and consequently enhanced the dehydration activity. It has been found that dehydration activity is related to the amount of surface acidity while the dehydrogenation of this alcohol is sensitive to NiO content.

Keywords: *NiO supported zirconia; acidity of solid catalyst; isopropanol conversion*



## 1. Introduction

Metal oxides have a wide range of industrial applications including chemical sensors, microelectronic materials, ceramics and catalysis. In heterogeneous catalysis, metal oxides can be used as either active catalysts or supports for dispersing catalytically active metal catalysts [1, 2].

Among various metal oxides, zirconia is of a particular interest and has received widespread attention due to its thermal stability and mechanical properties. Moreover, zirconia is claimed to be a good catalyst that has acidic, basic, reducing and oxidizing surface properties. In modern industry, zirconia has been widely used in various fields such as high-temperature fuel cells [3, 4], structural ceramics [5], gas sensors [6, 7], and as an insulator in metal oxide semiconductor devices [8, 9]. Zirconia was used also as a support and/or catalyst material with unique properties in a great variety of reactions. As a support, zirconia supported metal and metal oxides have been used in numerous catalytic reactions such as CO oxidation [10, 11], water gas shift reaction [12, 13] and selective hydrogenation of unsaturated organic compounds [14]. As an active catalyst component, zirconia has been used for catalytic reactions, such as alkene isomerization [15], alcohol dehydration [16] and hydrogenation and dehydrogenation of hydrocarbons [17]. Moreover, $ZrO_2$ can be used as a promoter to improve the catalytic performance of the catalysts, for example $ZrO_2$ additive improves the activity and thermal stability of Au/$FeO_3$ catalyst for low temperature water gas shift reaction [18].

Pure zirconia has three different crystal structures: monoclinic: m-$ZrO_2$, tetragonal: t-$ZrO_2$ and cubic: c-$ZrO_2$ [19]. It is worth noting that the method of preparation and its conditions (temperature and additives) greatly influence the phase structure of the synthesized zirconia and hence, significantly influence its physical properties. $ZrO_2$, when modified with sulfate ions, forms a highly

*E-mail: rehamfattah2012@gmail.com

acidic catalyst, stabilizing the tetragonal polymorph [20]. The acidic and catalytic properties of sulfated zirconia-based catalysts depend on a number of preparative parameters, among which particularly important are the nature of sulfation procedure, sulfating agent, precipitation procedure [21], thermal treatment, hydration degree and addition of transition metals as promoters [22, 23].

Numerous studies have also been devoted to NiO-based catalysts such as NiO–$AlO_3$ and NiO–$SiO_2$ systems which are widely used as catalysts for the oxidative dehydrogenation of ethane to ethylene, NO reduction by CO and $CH_4$–CO reforming. The surface properties and the catalytic performance of these catalyst systems have been reported [24–26].

The aim of the present work is to investigate the structural properties and thermal stability of $ZrO_2$ and NiO–$ZrO_2$ catalysts derived from NaOH–$Na_2C_2O_4$ assisted co-precipitation method. The effects of doping with fluoride ion and calcination temperatures on the structural, textural and acidic properties of $ZrO_2$ and NiO–$ZrO_2$ catalysts were also studied. The catalytic performance of the prepared catalysts towards isopropanol conversion was investigated.

# 2. Experimental

## 2.1. Catalyst preparation

Pure $Zr(OH)_4$ gel was prepared by a dropwise addition of $Na_2C_2O_4$–NaOH solution with mole ratio of 1/2 ($Na_2C_2O_4$, 0.5M) to an aqueous solution of $ZrOCl_2{\cdot}8H_2O$. Mixtures of $Zr(OH)_4$ and $Ni(OH)_2$ gels were prepared by co-precipitation from mixed solutions of $ZrOCl_2{\cdot}8H_2O$ and $NiCl_2{\cdot}6H_2O$ with $Na_2C_2O_4$–NaOH solution so as they contained 5, 10, 15 and 25 wt.% NiO, respectively. The dropwise addition of $Na_2C_2O_4$–NaOH solution was continued at 40 °C with vigorous stirring up to pH = 9. The resulting gels were separated by filtration, washing several times with bi-distilled water till free from chloride ions were obtained and drying at 100 °C for 24 h.

Two fluoride ion doped samples were also obtained by incipient wetness impregnation method. Pure $Zr(OH)_4$ and a sample containing 15 wt.% NiO were treated with ammonium fluoride solutions with fluoride content of 6 wt.%. The obtained pastes were dried at 100 °C for 24 h.

All the gels were calcined for 6 h at 550, 650, 750, and 850 °C, respectively. In the designation of the investigated samples, the letters Z, N, F denote $ZrO_2$, NiO and fluoride ion doped samples, respectively. The Roman numbers I, II, III and IV refer to the samples calcined at 550, 650, 750 and 850 °C, while the Arabic numbers 5, 10, 15 and 25 represent NiO wt.% loading. Accordingly, the designation ZN15FII refers to a $ZrO_2$–NiO sample containing 15 wt.% NiO, doped with fluoride ion and calcined at 650 °C.

## 2.2. Techniques of characterization

### 2.2.1. Thermal analysis

DTA analysis of various uncalcined samples was carried out using Shimadzu DTA-50 at a heating rate of 10 °C $min^{-1}$ in a flow of 30 mL·$min^{-1}$ $N_2$ gas.

### 2.2.2. X-ray diffraction (XRD)

X-ray powder diffraction (XRD) patterns of the calcined samples were recorded using PANalytical, X'Pert PRO diffractometer with nickel filtered CuK$\alpha$ radiation over the 2$\theta$ range of 2 ° to 80 °. The crystal sizes of the investigated samples were calculated from XRD line broadening using the Scherrer's equation [27]. The characteristic peaks at 2$\theta$ = 28.2 ° and 31.5 ° for ($\bar{1}$11) and (111) reflexes respectively were assigned to monoclinic phase in $ZrO_2$, while the peak at 2$\theta$ = 30.2 ° for the (111) reflex was assigned to tetragonal phase in $ZrO_2$.

The percentages of tetragonal and monoclinic phases in $ZrO_2$ were determined by means of their Gaussian areas "h × w" where h and w are the height and half-height width of the corresponding XRD characteristic peak using the following relations [28]:

$$\%\text{Monoclinic phase} = \frac{\sum(h \times w)_{m-ZrO_2\,\text{phase}(M)}}{\sum(h \times w)_{m-ZrO_2\,\text{phase}(M),t-Zr_2\,\text{phase}(T)}}$$

$$\%\text{Tetragonal phase} = \frac{\sum(h \times w)_{t-ZrO_2\,\text{phase}(T)}}{\sum(h \times w)_{m-ZrO_2\,\text{phase}(M),t-Zr_2\,\text{phase}(T)}}$$

### 2.2.3. Nitrogen physisorption

Nitrogen adsorption-desorption isotherms were measured at −196 °C using Quantachrome, Nova 3200. Samples were degassed under a vacuum of about 0.13 Pa for 2 h at 150 °C prior to the adsorption experiments. Specific surface areas were calculated using BET method ($S_{BET}$) and the existence of microporosity was tested from t-plot constructions.

### 2.2.4. Surface acidity measurements

The total acidity of the prepared samples was estimated by means of potentiometric n-butyl amine titration method [29]. 0.2 g of the catalyst was suspended in 20 mL of acetonitrile and stirred for 2 h. The electrode potential variation of the suspended sample with the addition of 0.025 M n-butyl amine was measured using an Orion 420 digital: a model with a double junction electrode. The addition was continued till no further change of mV was recorded.

### 2.2.5. Catalytic activity measurements

The catalytic conversion of isopropanol was carried out using a pulse microcatalytic system connected to a flame ionization detector (Hewlett Packard 5890A gas chromatograph). Prior to any catalytic run, the catalyst (100 mg) was activated for 30 minutes at the desired reaction temperature. Nitrogen was used as a carrier gas in all catalytic measurements and $1 \times 10^{-3}$ mL sample of isopropanol was injected to the catalyst in the form of pulse using a microsyringe.

## 3. Results and discussion:

### 3.1. Thermal analysis

The differential thermograms of fluoride ion undoped samples pre-dried at 90 °C are shown in Fig. 1. Evidently, two endothermic effects are exhibited by all the samples. The first endothermic effect shows its maximum between 95 and 110 °C and is attributed to the removal of physisorbed water. The second endothermic effect takes place between 245 and 280 °C leading to more developed peaks with their location shifted to higher temperatures with increasing NiO content. This endothermic effect may be related to the dehydroxylation of the two metal hydroxides. In case of NiO–$ZrO_2$ catalysts, NiO influences the phase transition of $ZrO_2$. Thus, Z sample (pure $Zr(OH)_4$) exhibits an exothermic effect at 437 °C. This effect is observed at 485, 558, 607 and 650 °C for ZN5, ZN10, ZN15 and ZN25, respectively, i.e. the position of the exotherm shifts to higher temperature with the increase in nickel oxide content. Moreover, the area of the peak characterizing this exothermic effect continuously decreases with the increase in NiO content. These exotherms may account for the crystallization of $ZrO_2$ to metastable tetragonal phase [30]. This new phase (t-$ZrO_2$)

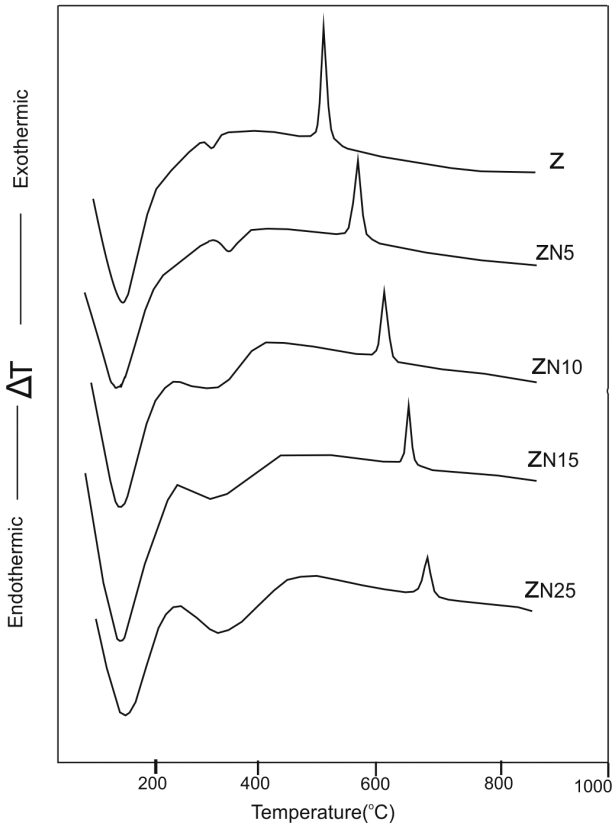


Fig. 1. DTA curves of Z, ZN5, ZN10, ZN15 and ZN25 gels.

has probably different specific heat compared with hydroxide.

The differential thermograms of ZF and ZN15F samples are shown in Fig. 2. Evidently, ZF and ZN15F samples show an additional endothermic effect at around 400 °C which may be attributed to the decomposition of ammonium salt. Moreover, for one and the same chemical composition the area of the exothermic peak characterizing the crystallization of $ZrO_2$ decreases due to the addition of fluoride ion.

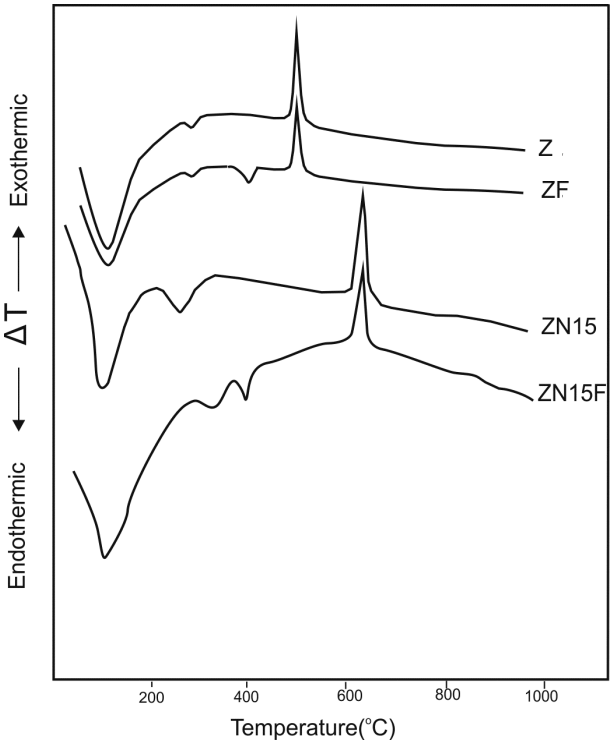


Fig. 2. DTA curves of Z, ZF, ZN15 and ZN15F gels.

## 3.2. Crystal structure

The XRD patterns of NiO–$ZrO_2$ samples calcined at 550 °C and those for Z and ZN15 samples calcined at different temperatures are illustrated in Fig. 3 to Fig. 5. The corresponding phase compositions are presented in Table 1 and Table 2. As seen from Fig. 3 to Fig. 5 the chemical composition and the calcination temperature show significant impact on both crystal phase and crystallite size. The degree of crystallinity of tetragonal phase

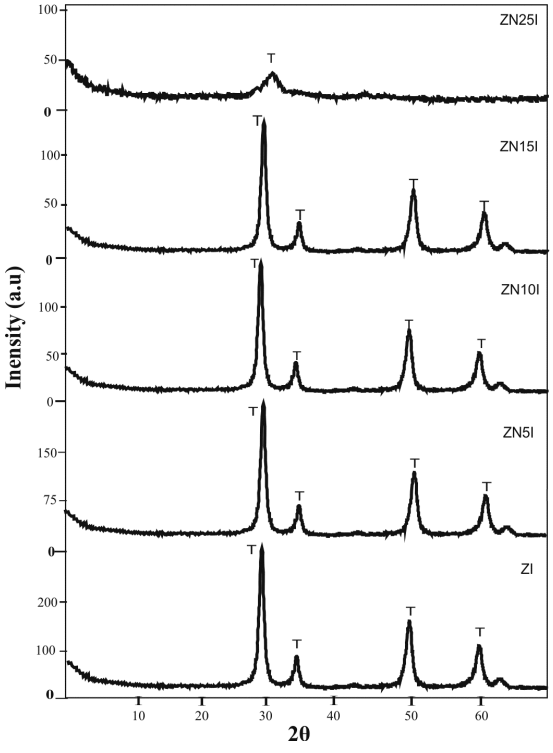


Fig. 3. XRD patterns of $ZrO_2$ and NiO–$ZrO_2$ samples calcined at 550 °C.

decreases gradually by increasing NiO content up to 25 wt.% (Fig. 3). It seems that the increase in NiO content to a certain limit is accompanied by crystallite growth and instability of the tetragonal phase. Most published studies agree that incorporation of some additive materials retards crystallization of zirconia, supporting and enhancing its amorphous structure [31, 32]. In fact, the tetragonal phase should be formed above 1170 °C, but in many cases, zirconia obtained by precipitation from aqueous salt solution occurs as a metastable tetragonal phase at lower temperature [33]. Moreover, the transformation of the metastable tetragonal phase into the monoclinic phase is probably due to the lower surface energy of the tetragonal phase compared to the monoclinic phase [34, 35]. Fig. 3 reveals also the absence of diffraction lines characteristic of NiO phase for all NiO–$ZrO_2$ samples calcined at 550 °C. This may be attributed to the high surface area of zirconia support which allowed the high dispersion of NiO species and inhibited the formation of NiO crystallites.

Table 1. Crystal structure and crystal size of undoped catalysts.

| Catalyst | Phases detected* | Major phase [%] | Crystal size (D) of major phase [nm] | Degree of crystallinity [a.u.]** | | $E_s$ [kJ·mol$^{-1}$] |
|---|---|---|---|---|---|---|
| | | | | M($2\theta = 28.2$) | T($2\theta = 30.3$) | |
| ZI | T | 100(T) | 29.5 | 225 | – | 13.8 |
| ZII | T | 100(T) | 38.0 | 268 | – | |
| ZIII | T | 100 (T) | 44.5 | 380 | – | |
| ZIV | M+T | 83.8(M) | 49.5 | 130 | 300 | |
| ZN5I | T | 100(T) | 19.5 | 210 | – | |
| ZN10I | T | 100(T) | 23.4 | 190 | – | |
| ZN15I | T | 100(T) | 29.5 | 145 | – | |
| ZN25I | T | 100(T) | 39.5 | 36 | – | |
| ZN15I | T | 100(T) | 29.5 | 145 | – | 24.89 |
| ZN15II | T | 100(T) | 21.4 | 282 | – | |
| ZN15III | M+T+C | 64.1(M) | 31.0 | 178 | 195 | |
| ZN15IV | M+T+C | 91.3(M) | 40.5 | 48 | 343 | |

*M: monoclinic $ZrO_2$, T: tetragonal $ZrO_2$ and C: cubic NiO.

**The peak height of the major line of each phase was taken as a measure of the degree of crystallinity of the $ZrO_2$.

Table 2. Crystal structure and crystal size of the samples doped with fluoride ions.

| Catalyst | Phases detected* | Major phase [%] | Crystal size [D] of major phase [nm] | Degree of crystallinity [a.u.]** | | $E_s$ [kJ·mol$^{-1}$] |
|---|---|---|---|---|---|---|
| | | | | M($2\theta = 28.2$) | T($2\theta = 30.3$) | |
| ZFI | T | 100 (T) | 30.0 | 280 | – | 13.21 |
| ZFII | T | 100 (T) | 36.8 | 265 | – | |
| ZFIII | T | 100 (T) | 42.0 | 290 | – | |
| ZFIV | M+T | 86.2(M) | 48.5 | 110 | 210 | |
| ZN15FI | T | 100 (T) | 18.0 | 130 | – | 23.16 |
| ZN15FII | T | 100 (T) | 22.0 | 212 | – | |
| ZN15FIII | M+T+C | 73.6(M) | 30.0 | 140 | 118 | |
| ZN15FIV | M+T+C | 85.5(M) | 41.0 | 24 | 160 | |

*M: monoclinic $ZrO_2$, T: tetragonal $ZrO_2$ and C: cubic NiO.

**The peak height of the major line of each phase was taken as a measure for the degree of crystallinity of $ZrO_2$.

The XRD patterns of Z and ZN15 samples calcined at different temperatures exhibit in some cases biphasic mixture of tetragonal and monoclinic phase as indicated in Fig. 4 and Fig. 5. It is interesting to note that the tetragonal phase transformation to the monoclinic one starts at 750 °C and increases with an increase of calcination temperature from 750 to 850 °C. In agreement with DTA results, the increase of the calcination temperature leads to crystallite growth due to the loss of water content, which leads to instability of tetragonal phase and then to the transition from the tetragonal phase to the monoclinic phase [36, 37]. Fig. 5 indicates also the absence of NiO diffraction lines for ZN15 sample calcined at $T \leqslant 650$ °C. This may be due to the high dispersion of NiO species and/or to its amorphous nature. Very weak reflection lines at $2\theta = 43.5$ °, 47 ° and 60 ° appear after calcination at $T \geqslant 750$ °C corresponding respectively to the planes of (1 1 1), (1 0 2) and (2 0 0) which can be assigned to the presence of trace amount of cubic NiO.

The XRD patterns of fluoride ion doped samples were also determined (not illustrated) and their results are summarized in Table 2. It can be seen from Table 1 and Table 2 that fluoride ion doped samples have slightly lower values of crystallite size and degree of crystallinity than undoped samples. Moreover, fluorinated samples show XRD patterns more or less similar to those of undoped Z and ZN15 samples. This means that addition

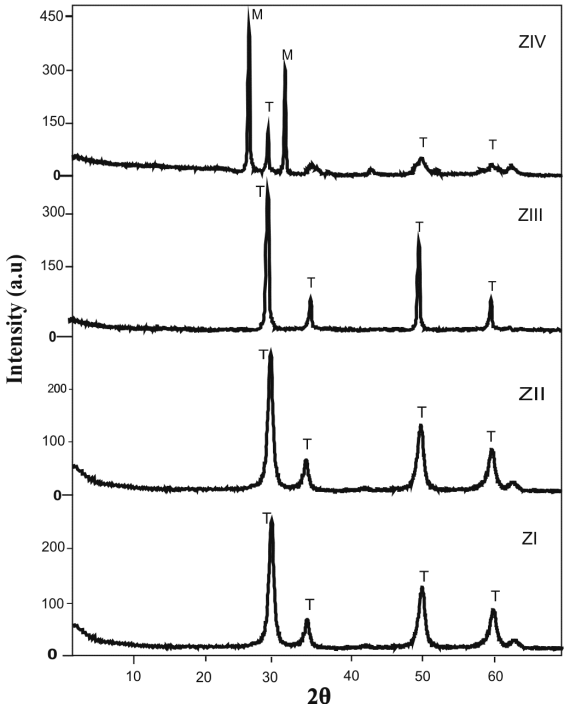


Fig. 4. XRD patterns of $ZrO_2$ sample calcined at different temperatures.

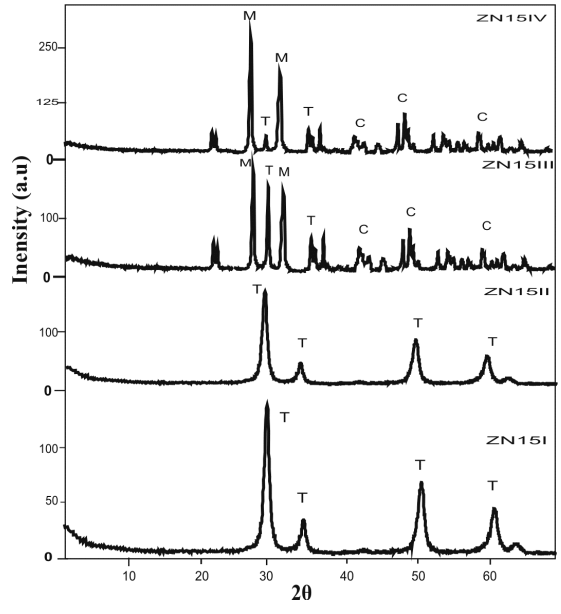


Fig. 5. XRD patterns of ZN15 sample calcined at different temperatures.

of fluoride ion dopant to Z and ZN15 samples slightly affects their structural characteristics.

Finally, it is worth noting that for one and the same chemical composition, the degree of crystallinity was found to increase with the increase of calcination temperature while for the samples calcined at 550 °C the degree of crystallinity decreased gradually with the increase in NiO content.

### 3.3. Textural properties

All the investigated samples showed more or less similar nitrogen adsorption isotherms. Although some minor changes have been observed, yet all the isotherms belong to type IV according to IUPAC [38], indicating thus the predominance of the mesoporous structure for all the samples. Representative adsorption-desorption isotherms are illustrated in Fig. 6. The textural parameters including specific surface area ($S_{BET}$, $m^2 \cdot g^{-1}$) and total pore volume ($V_p$, $mL \cdot g^{-1}$) were determined from the analysis of these isotherms. The main pore radius $\bar{r}$ (Å) was calculated from the relationship: $\bar{r}$ (Å) $= (2V_p \times 10^4)/S_{BET}$ The textural parameters $S_{BET}$, $V_p$ and $\bar{r}$ are listed in columns (2, 4 and 5) of Table 3.

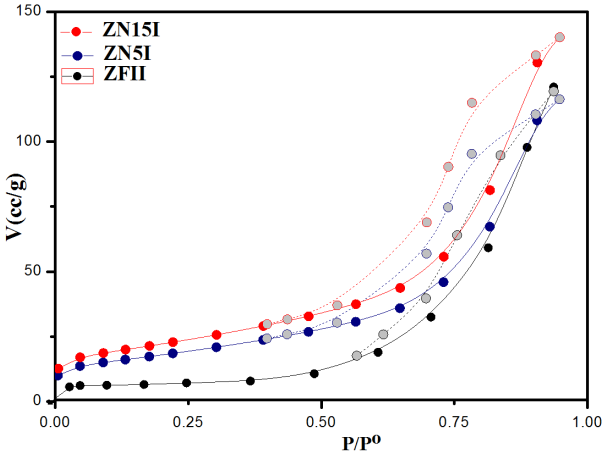


Fig. 6. Nitrogen adsorption-desorption isotherms of some selected samples.

The $V_l-t$ method suggested by de Boer was also employed to calculate the surface area, $S_t$ ($m^2 \cdot g^{-1}$) from the slope of the linear part of the $V_l-t$ plots which passes through the origin [39]. The calculated $S_t$ areas are compared with $S_{BET}$ areas in columns 3 and 2 of Table 3, respectively. The

$V_I$−t plots of all investigated samples (not illustrated) showed an upward deviation indicating the domination of the mesoporous structure for all the investigated samples. This conclusion is also supported by comparing the values of r̄ given in Table 3 which shows that the r̄ values of all samples vary between 30 and 96 Å.

Inspection of the textural data in columns 2 to 5 of Table 3 reveals the following:

1. The values of $S_{BET}$ and $S_t$ for all investigated samples are close to each other which justifies the correct choice of standard t curve used in the pore analysis.
2. For the samples calcined at 550 °C the surface area increases gradually upon increasing NiO content, reaching a maximum at 15 wt.% NiO. Further increase of NiO content beyond 15 wt.% was associated with a significant decrease in both the surface area and the total pore volume. At low NiO content up to 15 wt.%, two phenomena in principle could be acting. One is interconnection between original $ZrO_2$ grains with the incorporated NiO particles, while the other is simultaneous filling of $ZrO_2$ pores. During thermal treatment the two effects may lead to the creation of new mesopores as well as enhancing the disaggregation of the resulting particles. These effects could explain the increase of the surface area as observed in Table 3. At higher NiO content the NiO particles start to block some of the pores of the catalyst, thereby reducing the surface and the total pore volume.
3. Finally, for one and the same chemical composition, the surface area and the total pore volume decreased with increasing the calcination temperature from 550 to 850 °C. The increase of the calcination temperature led to crystallite growth due to the elimination of water content. This process caused the instability of tetragonal phase indicating the sintering of zirconia particles which resulted in the decrease of both $S_{BET}$ area and total pore volume. Fluoride ion undoped samples exhibit slightly higher values of surface parameters than the doped ones.

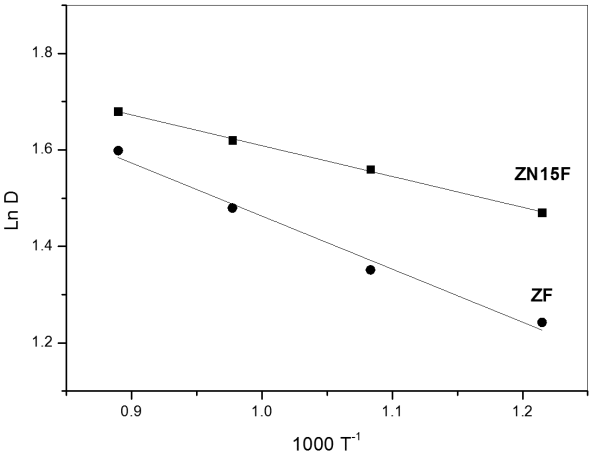


Fig. 7. Arrhenius plots of activation energy of sintering process for tested samples.

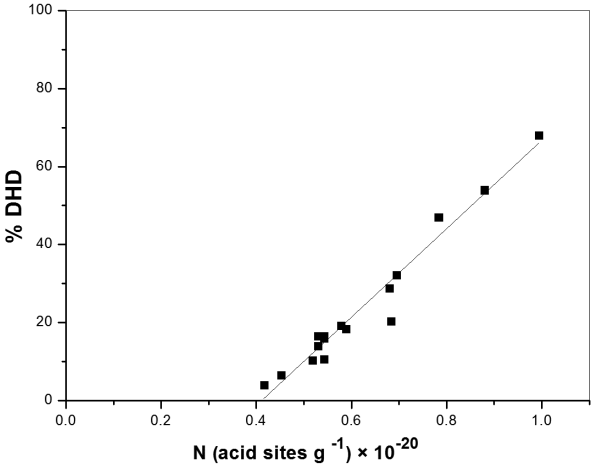


Fig. 8. DHD of isopropanol as a function of acid sites per gram for ZI sample.

It is interesting to show how the crystallite size of initial grains of zirconia is affected by the thermal treatment, where the grains growth of the prepared particles takes place. After crystallization, the particles continue to increase in size with increasing calcination temperature through the process of sintering, which is confirmed by the increased intensity of the XRD diffraction lines. The variation of the crystallite size (D) of t-$ZrO_2$ phase calculated from its XRD line broadening with

Table 3. Surface characteristics, acidic and catalytic properties of the investigated catalysts.

| Sample | $S_{BET}$ [$m^2 \cdot g^{-1}$] | $S_t$ [$m^2 \cdot g^{-1}$] | $V_p$ [$ml \cdot g^{-1}$] | $\bar{r}$ [Å] | $E_i$ [mV] | N (acid sites $g^{-1}$) $\times 10^{-20}$ | DHD [%] | DHG [%] |
|---|---|---|---|---|---|---|---|---|
| ZI | 76.03 | 70.5 | 0.21 | 54.4 | 41 | 0.72 | 37.3 | 0 |
| ZII | 58.0 | 58.2 | 0.18 | 56.7 | 35 | 0.680 | 28.8 | 0 |
| ZIII | 50.6 | 28.4 | 0.13 | 72.2 | 30 | 0.590 | 18.4 | 0 |
| ZIV | 18 | 11.8 | 0.09 | 96.0 | 13 | 0.518 | 10.4 | 0 |
| ZN5I | 98.6 | 100.2 | 0.34 | 96.08 | 52 | 0.578 | 20.4 | 14.6 |
| ZN10I | 127.6 | 130.4 | 0.38 | 71.37 | 62 | 0.530 | 19.2 | 20.4 |
| ZN15I | 138.0 | 144.0 | 0.342 | 53.46 | 70 | 0.542 | 16.5 | 28.6 |
| ZN25I | 100.0 | 98.0 | 0.159 | 31.0 | 78 | 0.430 | 10.6 | 38.0 |
| ZN15I | 138.0 | 144.0 | 0.342 | 53.46 | 70 | 0.542 | 16.5 | 28.6 |
| ZN15II | 80.0 | 78.6 | 0.26 | 59.8 | 71 | 0.542 | 16.0 | 27.8 |
| ZN15III | 36.0 | 34.4 | 0.18 | 68.53 | 56 | 0.452 | 6.6 | 9.6 |
| ZN15IV | 20.4 | 18.0 | 0.114 | 72.0 | 44 | 0.380 | 4.0 | 6.0 |
| ZFI | 70.6 | 69.5 | 0.206 | 58.3 | 81 | 0.994 | 68.0 | 0 |
| ZFII | 50.4 | 49.0 | 0.189 | 75.0 | 72 | 0.78 | 47.0 | 0 |
| ZFIII | 27.8 | 31.0 | 0.14 | 90.3 | 63 | 0.693 | 32.3 | 0 |
| ZFIV | 12.4 | 20.4 | 0.102 | 113 | 66 | 0.530 | 14.0 | 0 |
| ZN15FI | 118.0 | 117.6 | 0.306 | 51.8 | 98 | 0.879 | 54.0 | 12.0 |

the preheating temperature, T (550 to 850 °C) permits the calculation of activation energy of sintering ($E_s$) of t-$ZrO_2$ phase using Arrhenius equation:

$$D = Ae^{-E_s/RT}$$

where A is the frequency factor of Arrhenius equation and $E_s$ is the activation energy of sintering process of the sample [40]. By plotting ln D versus 1/T, a straight line is obtained whose slope and intercept permit the calculation of $E_s$ and A. The Arrhenius plots for undoped and fluoride ion doped Z and ZN15 samples are shown in Fig. 7. The calculated $E_s$ values are 13.8 and 24.9 $kJ \cdot mol^{-1}$ for the Z and ZN15 samples, respectively. These results suggested that pure zirconia responds to sintering faster than NiO supported samples. One can conclude that incorporation of NiO into $ZrO_2$ matrix led to improving its thermal stability. The obtained $E_s$ values of the two samples after doping with fluoride ions were found to be 13.21 and 23.16 $kJ \cdot mol^{-1}$, respectively. It seems that the addition of fluoride ions slightly decreased the thermal stability of the two samples. These results complement also the results obtained from XRD data and confirm that with the increase of calcination temperature, and consequently the increase of crystallite size, was the reason for the pronounced decrease in BET surface area of the calcined samples.

### 3.4. Surface acidity

As a criterion to interpret the obtained results, it has been assumed that the initial electrode potential ($E_i$) indicates the maximum acid strength of the acid sites, and the value of $ml_{eq.amine}$ per gram solid, where the plateau of titration curve is reached, indicates the total acidity [41]. Moreover, the acid strength of these sites can be classified according to the following scale: ($E_i > 100$ mV) very strong sites, ($0$ mV $< E_i <$ 100 mV) strong sites, ($-100$ mV $< E_i < 0$ mV) weak sites and ($E_i < -100$ mV) very weak sites [42]. The values of $E_i$ and the total number of acid sites per gram catalyst are listed in columns 6 and 7 of Table 3. Generally, the total acidity expressed as a number of acid sites per gram catalyst, N (acid sites $g^{-1}$) continuously decreases with the rise of calcination temperature. Probably the rise of calcination temperature partially removes a fraction of surface acid sites. This was the case for all the catalysts under investigation. It is also evident that the number of acid sites per gram continuously decreases with the increase in NiO content. On contrary,

the acid strength as indicated from the $E_i$ values was found to increase with the increase in NiO content. This may be taken as an evidence that NiO removes weak acid sites and concentrates the strong ones. Finally, the ZFI sample shows the highest acid amount among the other samples while the ZN15IV shows the lowest one.

### 3.5. Conversion of isopropanol

Conversion of isopropanol proceeds through two main reaction paths, namely dehydration (DHD) to propene and dehydrogenation (DHG) to acetone. DHD proceeds on acid sites [43], while DHG is related to the P-type conductivity and the electronic characteristics of the solid catalyst [44]. The percentage of DHD and DHG activities at 300 °C and at a flow rate of the nitrogen carrier gas of 25 mL·min$^{-1}$ are listed in columns 8 and 9 of Table 3.

The data in this table indicate that: (i) NiO–$ZrO_2$ catalysts reveal DHD and DHG activities while $ZrO_2$ catalysts shows only DHD activities. (ii) In general, the DHD activities decrease while the DHG activities increase with increasing NiO content. (iii) The DHD activities of ZI samples markedly increase with fluoride ion doping. The observed increase in the DHD activity of pure $ZrO_2$ sample due to doping with fluoride ion reflects an effective increase in the concentration of the surface acid sites which represent the catalytically active sites for the dehydration of alcohols. (iv) Finally, for one and the same chemical composition (i.e. for ZN15 sample) the DHD and DHG activities remain approximately constant with an increase in calcination temperature in the range of 550 to 650 °C and then they decrease with further temperature increase up to 850 °C. This finding may be attributed to restriction of catalytic active constitutes due to partial removal of a fraction of surface acidities, increasing the degree of crystallinity of detected phases and sintering process.

No relation was found between either the DHD or DHG activities on the one hand and the total $S_{BET}$ areas on the other hand. The results reveal also that DHD activity is not sensitive to the strength of the acid sites. This is indicated by a significant DHD activity of ZI sample which has a low value of acid strength ($E_i = 41$ mV). Moreover, NiO–$ZrO_2$ samples show lower values of DHD activity although they have relatively higher values of acid strength ($E_i = 44$ to 78 mV) in comparison with that of pure $ZrO_2$. Evidently dehydration of this alcohol was found related to the number of acid sites per gram where straight line was obtained between the percentage of DHD activity and N (acid sites g$^{-1}$) (Fig. 8). Extension of the straight line in Fig. 8 intersects the N (acid sites) axis indicating that a minimum number of acid sites per gram catalyst are necessary to initiate dehydration of isopropanol. It seems that dehydration of isopropanol is related to the number of acid sites on the surface of the catalyst rather than to the strength of these acid sites, which agrees well with previous studies [45, 46].

## 4. Conclusions

Stabilization of the t-$ZrO_2$ phase was maintained upon calcination up to $T \leqslant 750$ °C. Thermal treatment at $T > 750$ °C resulted in phase transformation from tetragonal to monoclinic zirconia due to the increase of crystallite size above the critical size of tetragonal phase. The addition of NiO to $ZrO_2$ influenced the phase transition of $ZrO_2$. No spinel structure was detected by both DTA and XRD techniques and only trace amounts of c-NiO were detected for the samples containing $\geqslant$ 15 wt.% NiO calcined at $T \geqslant 750$ °C. The crystallite size of initial grains of $ZrO_2$ was affected by the thermal treatment where the size of the crystal increased with an increase in calcination temperature due to sintering process. The results agree well with those obtained from XRD data and confirm that the increase in the crystallite size was the reason for the pronounced decrease in BET surface area upon increasing temperature. Fluoride ion doping slightly affected the structure and texture properties of the doped samples but rather markedly increased the degree of surface acidity which represents the catalytically active constituents taking part in the DHD of alcohol. Pure and fluoride ion doped zirconia catalysts exhibit no DHG activity, whereas

supported with NiO favored the conversion of isopropanol to propene and acetone. DHD to propene is related to the number of acid sites per unit weight while DHG to acetone is sensitive to NiO content.

## References


[1] CHEN M.S., GOODMAN D.W., *J. Phys. Condens. Matter.*, 20 (2008), 4013.

[2] SHAIKHTDMOV S., FREUND H., *Annu. Rev. Phys. Chem.*, 63 (2012), 619.

[3] JACOBSON A., *Chem. Mater.*, 22 (2010), 660.

[4] LAGUNA-BERCERO M.A., *J. Power Sources*, 203 (2012), 4.

[5] AKBAR S., DUTTA P., LEE C.H., *Appl. Ceram. Technol.*, 3 (2006), 302.

[6] FERGUS J.W., *Sensor. Actuat. B-Chem.*, 121 (2007), 652.

[7] KOROTECENKOV G., DOHAN S., STETTER J.R., *Chem. Rev.*, 109 (2009), 1402.

[8] STEMMER S., *J. Vac. Sci. Technol. B*, 22 (2004), 791.

[9] CHIANG C.K., WU C.H., LIU C.C., LIN J.F., YANG C.L., WU J.W., WANG S.J., *Jpn. J. Appl. Phys.*, (2012), 51.

[10] ZHANG X., SHI H., XU B.Q., *Catal. Today*, 122 (2007), 330.

[11] COMOTTI M., LI W.C., SPLIETHOFF B., SCHUTH F., *J. Am. Chem. Soc.*, 128 (3) (2006), 917.

[12] IDAKIEV V., TABAKOVA T., NAYDENOV A.Z., YUAN Y., SU B.L., *Appl. Catal. B-Environ.*, 63 (2006), 178.

[13] LI J., TA N., SONG W., ZHAN E.S., SHEN W.J., *Gold Bull.*, 42 (2009), 48.

[14] ZHANG X., SHI H., XU B.Q., *Angew. Chem. Int. Edit.*, 44 (2005), 7132.

[15] NAKANO Y., IIZUKA T., HATTORI H., TANABE T., *J. Catal.*, 57 (1979 ), 1.

[16] FERINO I., CASULA M.F., CORRIAS A., CUTRUFELLO M.G., MONACI R., PASCHINA G., *Phys. Chem. Chem. Phys.*, 2 (2000), 1847.

[17] TANABE K., YAMAGUCHI T., *Catal. Today*, 20 (1994), 185.

[18] ZHANG F., ZHENG Q., WEI K., LIN X., ZHANG H., LI J., CAO Y., *Catal. Lett.*, 108 (2006), 131.

[19] MUNOZ M. C., GALLEGO S., BELTRAN J.I., CERDA J., *Surf. Sci. Rep.*, 61 (2006), 303.

[20] BENITEZ J.J., ALVERO R., CARRIZOSA I., ODRIOZOLA J.A., *Catal. Today*, 9 (1991), 53.

[21] COMELLI R.A., VERA C.R., PAVERA J.M., *J. Catal.*, 151 (1995), 96.

[22] YADAV G.D., MURKUTE A.D., *J. Catal.*, 24 (2004), 218.

[23] BOLIS V., MAGNACCA G., CERRATO G., MORTERRA C., *Top. Catal.*, 19 (2002), 259.

[24] ZHANG X., LIU J., JING Y., XIE Y., *Appl. Catal. A-Gen.*, 240 (2003), 143.

[25] ANGELIDIS T.N., PAPAPETROU M., *Stud. Surf. Sci. Catal.*, 133 (2001), 131.

[26] CHEN X., HONDA K., ZHANG Z., *Appl. Catal. A-Gen.*, 288 (2005), 86.

[27] CULLITY B.D., *Elements of X-ray Diffraction*, Addison-Wesley, California, 1978.

[28] SU C., LI J., HE D., CHENG Z., ZHU Q., *Appl. Catal. A-Gen.*, 202 (2000), 81.

[29] RAO K.N., REDDY K.M., LINGAISH N., SURYANARAYANA I., PRASAD P.S., *Appl. Catal. A-Gen.*, 300 (2006), 139.

[30] LI G., LI W., ZHANG M., TAO K., *Catal. Today*, 93 – 95 (2004), 595.

[31] AHMED A.I., EL HAKAM S.A., SAMRA S.E., E-KHOLY A.A., KHDER A.S., *Colloid. Surface A*, 317 (2008), 62.

[32] SOHN J.R., PARK W.C., *Appl. Catal. A-Gen.*, 230 (2002), 11.

[33] FARCASIU D., LI J.Q., CAMERON S., *Appl. Catal. A-Gen.*, 154 (1997), 173.

[34] TANI E., YOSHIMURA M., SOMIYA S., *J. Am. Ceram. Soc.*, 66 (1983), 11.

[35] OSENDI M.I., MOYA J., SERNA C.J., SORIA J., *J. Am. Ceram. Soc.*, 68 (1985), 135.

[36] YAMAGUCHI T., TANABE T., *Mater. Chem. Phys.*, 16 (1987), 67.

[37] SRINIVASON R., KEOG R A., MILBURN D R., DAVIS B.H., *J. Catal.*, 153 (1995), 123.

[38] XU R.R., BANG W.Q., *Chemistry of molecule sieves and mesoporous materials*, Science Press, Beijing, 2004, p. 173.

[39] DE BOER J.H., *The structure and preperties of porous materials*, Butterworth, London, 1958.

[40] MOKHTAR M., BASAHL S.N., ALI T.T., *J. Mater. Sci.*, 48 (2013), 2705.

[41] PIZZIO L., VAZQUEZ P.G., CACERES C.V., BLANCO M.N., *Catal. Lett.*, 93 (2004) 67.

[42] PIZZIO L., BLANCO M.N., *Appl. Catal. A-Gen.*, 255 (2003), 265.

[43] MOSTAFA M.R., YOUSSEF A.M., *Mater. Lett.*, 34 (1998), 405.

[44] PEPE F., ANGELETTI C., ROSSI S.D., *J. Catal.*, 118 (1989), 1.

[45] MOSTAFA M.R., YOUSSEF A.M., HASSAN S.M., *Mater. Lett.*, 12 (1991), 207.

[46] MOSTAFA M.R., *Afinidad*, 51 (1994), 445.


*Received 2015-03-30*
*Accepted 2015-11-16*